

Developing Turbulent Forced Convection in Two-Dimensional Duct

Y. T. Chen¹

J. H. Nie

Department of Mechanical Engineering,
University of Nevada,
Las Vegas, NV 89154

B. F. Armaly

Department of Mechanical and Aerospace Engineering,
University of Missouri-Rolla,
Rolla, MO 65401

H. T. Hsieh

R. F. Boehm

Department of Mechanical Engineering,
University of Nevada,
Las Vegas, NV 89154

Developing turbulent forced convection flow in a two-dimensional duct is simulated for Reynolds numbers ranging from 4560 to 12,000. Simultaneously developing velocity and temperature distributions are reported by treating the inlet flow as isothermal with uniform velocity profile. The walls are supplied with uniform heat flux. Distributions of the streamwise and the transverse velocity components exhibit a maximum near the walls, but not at the center of the duct, in the developing region of the flow. The friction coefficient and the Nusselt number do not reach the fully developed values monotonously, and a minimum in their distributions appears in the developing region. Some results are compared with the available data, and very favorable comparisons are obtained. [DOI: 10.1115/1.2740659]

Keywords: turbulent, heat transfer, forced convection, developing flow, duct

Introduction

The fundamental turbulent flow and heat transfer mechanism is of great importance from both scientific and engineering viewpoints because it occurs frequently and plays a predominant role in convective momentum, heat and mass transfer in many industrial applications, such as compact heat exchangers, gas turbine cooling systems, nuclear reactors, and numerous others. Turbulent forced channel flow, due to its geometric simplicity and fundamental nature to understand the transport mechanism, has been studied extensively from both experimental [1–3] and numerical [4–6] approaches. Wei and Willmarth [2] presented the velocity components for the Reynolds numbers of 3000–40,000 using laser Doppler anemometer. The measurements using hot-film anemometry were reported by Johansson and Alfredsson [3]. During the recent years, the performance of turbulence and heat transfer models in predicting the velocity and temperature fields of relevant industrial flows has become increasingly important. Recent ad-

vances in large-scale computers have made it possible to conduct the fundamental studies of turbulent flow numerically at moderate Reynolds numbers. Kim et al. [4] numerically solved the unsteady Navier-Stokes equations using direct numerical simulation (DNS) at Reynolds number of 3300. A number of statistical correlations which were complementary to the existing experimental data were reported. Moser et al. [5] simulated the fully developed channel flow for the friction Reynolds number of 180–590 using direct numerical simulation. Abe et al. [6] reported the effects of Reynolds number on various turbulent statistics for the friction Reynolds numbers of 180, 395, and 640.

These experimental/numerical results are restricted to the fluid mechanics case. Kim and Moin [7] studied the heat transfer (mass transport) in two-dimensional forced convection channel flow for different Prandtl (Schmidt) numbers. Kasagi et al. [8] revisited the problems by employing a constant time-averaged heat flux boundary condition on the walls for a mild Reynolds number of 4580. Recently, Debusschere and Rutland [9] investigated the transport of passive heat transfer in a plane channel and Couette flow for the Reynolds number of 3000.

However, most of the published results are limited to the fully developed turbulent channel flow and/or the Reynolds number is mild. To the best of the authors' knowledge, study of simultaneously developing turbulent convection flow in channel has not been reported in the published literature. This fact, together with the realization that in the practical applications the flow and heat transfer start with the developing region and the Reynolds number is high, motivated the present study.

Problem Statement and Simulation Procedures

Turbulent developing forced convection flow in a parallel channel is numerically simulated. The simulated geometry has a height (h) of 0.01 m. By exploiting the symmetry of the flow and temperature fields in the transverse direction, the computational domain was reduced to half of the actual height of the channel ($\delta = 0.005$ m). This assumption of symmetry is confirmed by computation with a whole domain. The length of the computational domain is 2 m, i.e., $x/\delta \leq 400$. This computational domain was used in order to obtain the asymptotic behavior for the fully developed regime. The origin of the coordinates system is located at the bottom edge and the inlet of the channel. The steady turbulent Navier-Stokes and energy equations are solved numerically together with the continuity equation using the finite volume method and four-equation low-Reynolds-number model [10,11]. The governing equations based on the approximation of eddy-viscosity for fluid and eddy-diffusivity for heat and the constants appearing in the governing equations can be found in Ref. [12]. They are not shown here due to space limitation. The physical properties are treated as constants and evaluated for air at the inlet temperature (T_0) of 20°C, that is, density (ρ) is 1.205 kg/m³, molecular dynamic viscosity (μ) is 1.82×10^{-5} kg/(m s), specific heat (C_p) is 1005 J/(Kg°C), and thermal conductivity (λ) is 0.0258 W/(m°C). Flow at the inlet section of the channel ($x/\delta = 0$) is considered to be isothermal ($T_0 = 20^\circ\text{C}$), with a uniform streamwise velocity component (u) equal to the bulk velocity (u_0). The other velocity component, v , is set to be equal to zero at that inlet section. No slip boundary condition (zero velocities) is applied to the wall surface. Uniform heat flux ($q_w = 500$ W/m²) is applied at the walls. The kinetic energies (k and \bar{v}^2) at the wall are equal to zero. The dissipation rate for the fluid field (ε) is set to be $\varepsilon_w = 2\nu k_1/n_1^2$ and the dissipation rate for the thermal field (ε_t) is $\varepsilon_t = \alpha(\partial\sqrt{\bar{v}^2}/\partial n)^2$ at the solid walls, where k_1 is the kinetic energy and n_1 is the normal distance of the first node near the wall, respectively, and α is thermal diffusivity. Fully developed flow and thermal boundary conditions are imposed at the exit section of the computational domain ($x/\delta = 400$).

¹Corresponding author.

Contributed by the Heat Transfer Division of ASME for publication in the JOURNAL OF HEAT TRANSFER. Manuscript received December 28, 2005; final manuscript received October 24, 2006. Review conducted by N. K. Anand.

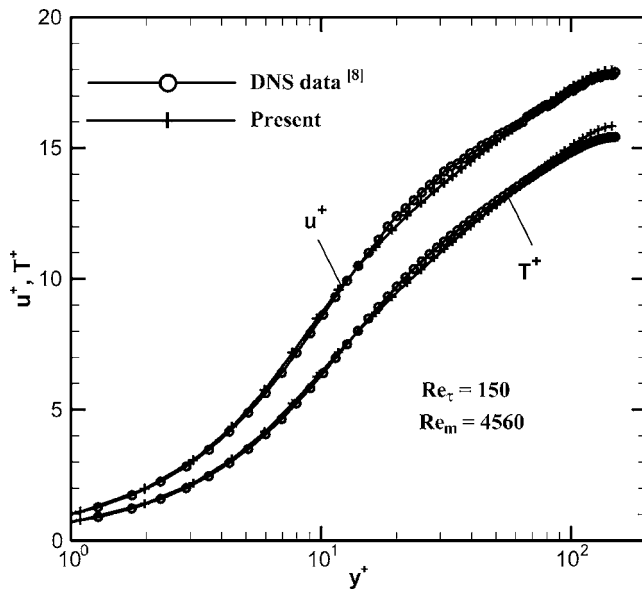


Fig. 1 Comparisons with the DNS data for the mean profiles

The governing equations are discretized using the staggered grid arrangement, and the resulting finite volume equations using SIMPLE algorithm are solved numerically by making use of a line-by-line method combined with ADI scheme [13]. Nonuniform grid system is employed in the simulations, and the grid is highly concentrated near the solid wall, in order to ensure the accuracy of the numerical simulations. Comparisons of the dimensionless mean velocity ($u^+ = u/u_\tau$, where $u_\tau = \sqrt{\tau_w/\rho}$ and τ_w is wall shear stress) and temperature [$T^+ = (T_w - T)/t_\tau$, where T_w is wall temperature and $t_\tau = q_w h / (\rho C_p u_\tau)$] profiles with the direct simulated data [8] are shown in Fig. 1. These profiles are taken at the streamwise location of $x/\delta = 390$, where the flow and heat transfer have already become fully developed. The mean velocity and temperature profiles agree closely well with those DNS results. Results from several grid densities for a Reynolds number ($Re_m = 2\rho u_m \delta / \mu$) of 6000 were used in developing a grid independence solution for this study. The velocity and temperature values at a selected point in the flow domain are presented in Table 1 for different computational grids. A grid of $100(x) \times 41(y)$ is used during the present simulations and a denser grid of $120(x) \times 51(y)$ results in less than 1% difference in the predicted streamwise velocity component at the selected point. The convergence criterion required that the maximum relative mass residual based on the inlet mass be smaller than 3×10^{-6} . It usually takes about 45,000 iterations to meet this requirement. The other test case to validate the flow simulation code that is used in this study is the two-dimensional turbulent flow and heat transfer over backward-facing step [12]. Predicted velocity profiles at several streamwise locations are compared with the laser Doppler measurements [14] as shown in Fig. 2 with good agreement between the predicted

Table 1 Velocities and temperatures at $x=0.2$ m and $y=0.002$ m for different computational grids ($Re_m=6000$)

Grid	Size ($x \times y$)	u (m/s)	v (m/s)	T ($^{\circ}\text{C}$)
1	40 \times 11	9.294	0.001381	22.26
2	60 \times 21	9.429	0.002070	22.14
3	80 \times 31	9.457	0.002196	22.10
4	100 \times 41	9.465	0.002218	22.08
5	120 \times 51	9.471	0.002231	22.07

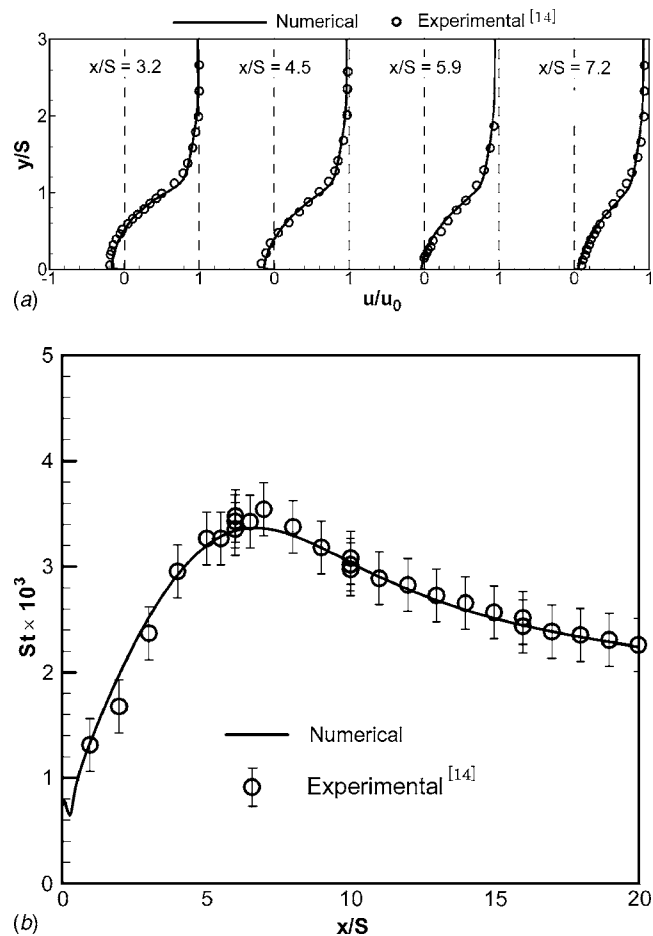


Fig. 2 Comparisons of the mean velocity profiles and the Stanton number for the separated convection flow

and measured data (S is step height). Comparison of the computed Stanton number [$St = q_w / (\rho C_p u_c (T_w - T_0))$], where u_c is the centerline velocity) on the heated bottom wall is made with the available measured data [14] as shown in Fig. 2. Very close agreement is obtained for the Stanton number profile inside the recirculation region and near the reattachment region, which justifies the present convection flow simulation code and provides with confidence for the next simulations.

Results and Discussions

The simultaneously developing turbulent flow and heat transfer in a parallel channel is simulated for different Reynolds numbers of 4560, 6000, 7500, 9000, 10,500 and 12,000. The bulk Nusselt number [$Nu_b = q_w h / \lambda (T_w - T_b)$, where T_b is bulk temperature] for the fully developed turbulent channel flow with a constant heat flux is shown in Fig. 3. The direct simulated result [8] and the experimental data [15] are also included in Fig. 3. The Nusselt number increases with the increase of Reynolds number. The Nusselt number obtained by the present simulation for $Re_m=4560$ is 15.5, and it is in excellent agreement with the DNS data which is 15.4 [8].

Distributions of the mean streamwise velocity component (u) at different streamwise locations in the entrance region of the channel are shown in Fig. 4 for the Reynolds numbers of 4560 and 12,000. Similar results are also obtained for other Reynolds numbers but not presented in the manuscript due to space limitation. Velocity at the centerline of the channel increases from the uniform inlet velocity profile to the fully developed velocity profile. The nonparabolic pattern observed for the laminar flow in a cir-

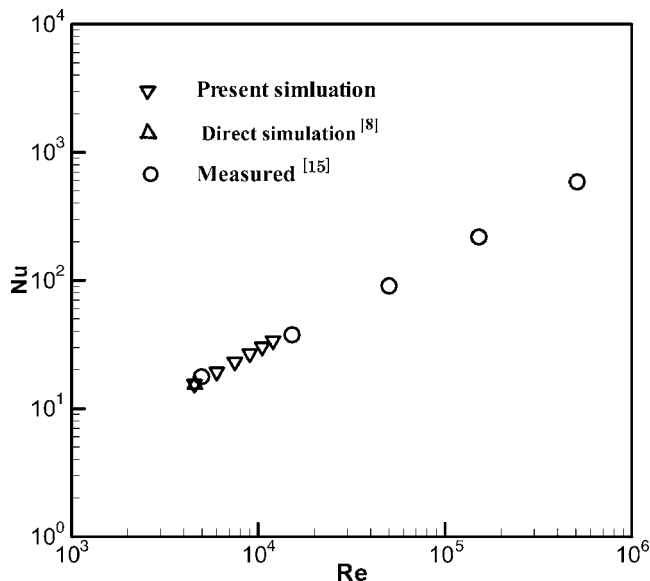


Fig. 3 Distribution of the Nusselt number for the fully developed turbulent channel flow

ular duct [16] is also seen for the turbulent flow in the parallel channel. In the entrance region, the maximum streamwise velocity component does not appear at the center of the channel, but near the solid wall ($y/\delta=0$). For the Reynolds numbers of 4560 and 12,000, at $x/\delta=1$, their peak values develop at $y/\delta \approx 0.16$ and 0.11, respectively. The similar feature can also be seen at the section of $x/\delta=0.5$. Distributions of the streamwise velocity component in the entrance region are displayed in Fig. 5. The dashed line denotes the locations where the streamwise velocity component (u) is a maximum at the streamwise planes. Figure 5 also shows that in the entrance region the maximum of this velocity component does not appear at the center of the channel, but near the wall.

Distributions of the transverse velocity component (v) at several streamwise locations for the Reynolds numbers of 4560 and 12,000 are shown in Fig. 6. The dashed line denotes the locations where the transverse velocity component (v) is a maximum at the streamwise planes. This velocity component is zero at the wall ($y/\delta=0$) and the symmetry centerline ($y/\delta=1$). For $Re_m=4560$ and 12,000 at $x/\delta=1$, their maximum values develop at $y/\delta \approx 0.12$ and 0.09, respectively. Its magnitude decreases and its location moves toward the centerline as the x -planes increase in the streamwise direction. At the same x -planes, the magnitudes of the peak v -velocity component decrease as the Reynolds number increases. Distributions of the transverse velocity component in the entrance region are presented in Fig. 7. The locations where the transverse velocity component is a maximum in the transverse direction for the x -planes are shown in Fig. 7 with the dashed lines. Near the inlet section, the maximum v -velocity component develops to appear close to the wall ($y/\delta=0$). Its location moves toward the centerline of the channel as the location of the x -plane increases in the flow direction.

Distributions of the temperature difference based on the wall temperature ($\delta T = T_w - T$) at several streamwise planes are shown in Fig. 8 for the Reynolds numbers of 4560 and 12,000. At the same streamwise planes, the temperature difference decreases as the Reynolds number increases. One feature in the temperature distribution is that the temperature difference increases at first from the inlet section ($x/\delta=0$) to the downstream section of $x/\delta=20$, then it decreases at the downstream x -planes (from $x/\delta=40$ to 100). The results show that profiles of the temperature difference at other downstream x -planes ($x/\delta > 100$) are almost

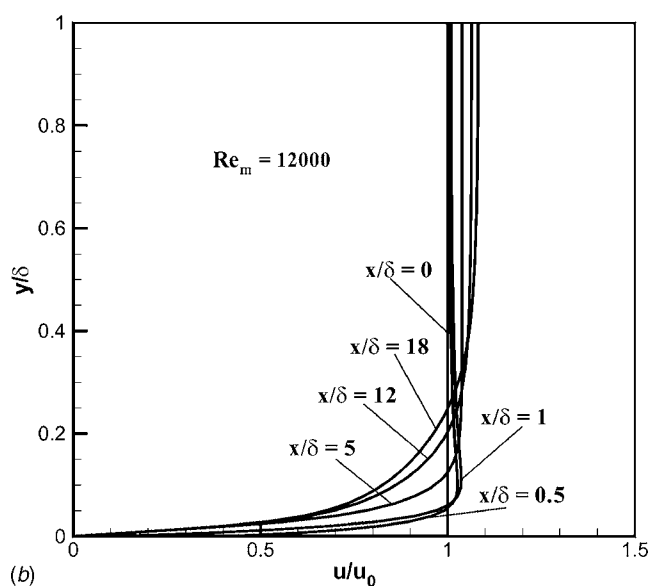
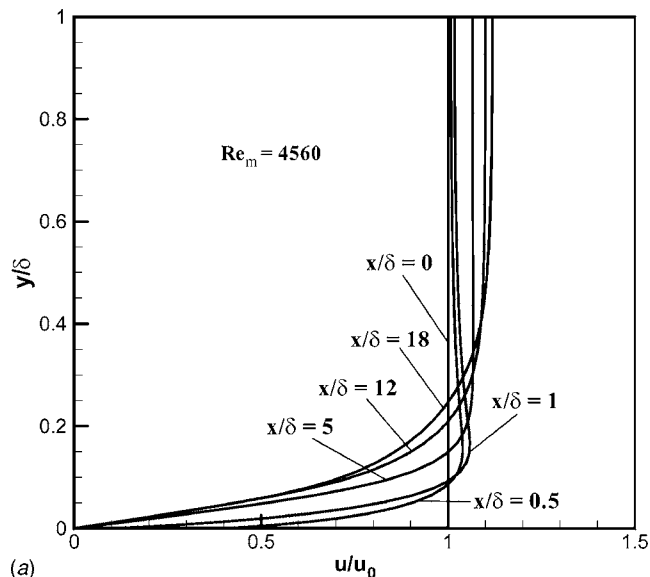


Fig. 4 Distributions of the streamwise velocity at several x -planes

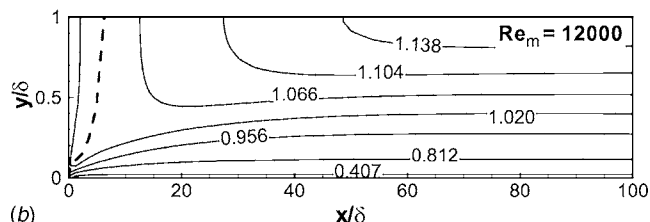
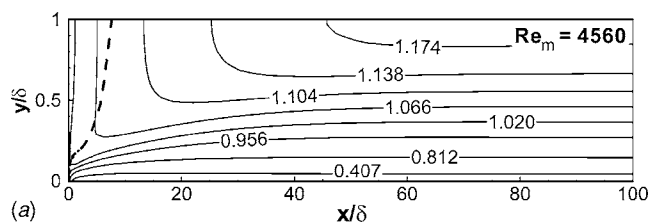
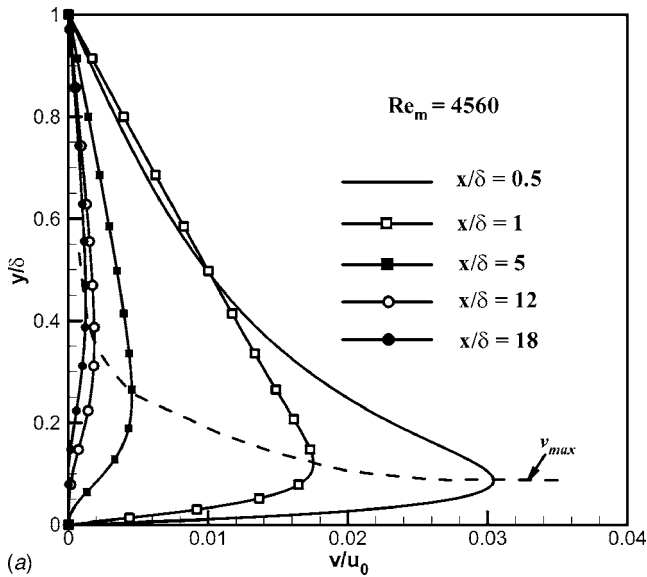
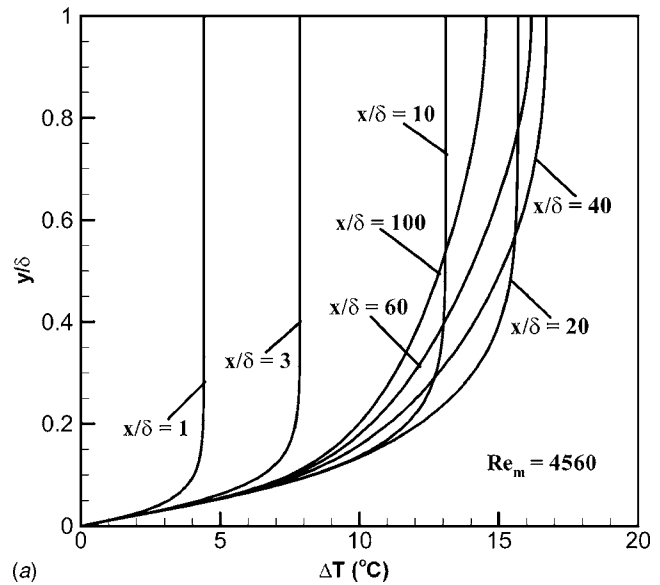


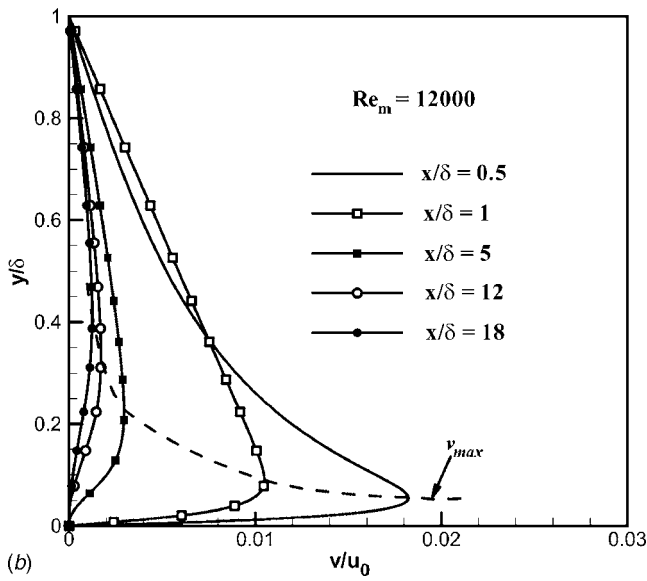
Fig. 5 Distributions of the streamwise velocity component (u)



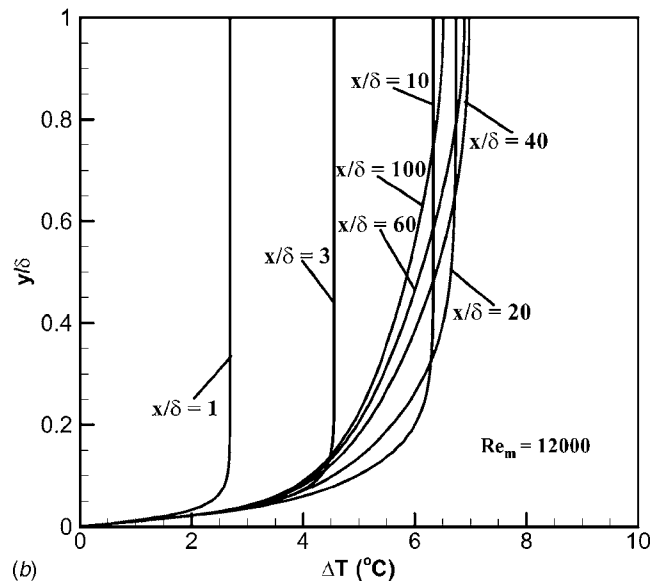
(a)



(a)



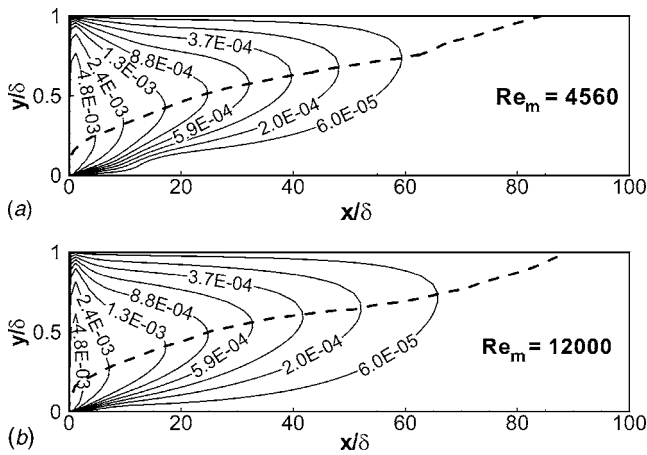
(b)



(b)

Fig. 6 Distributions of the transverse velocity component at several x -planes

Fig. 8 Distributions of the temperature difference ($T_w - T$) at several x -planes



(a)

(b)

Fig. 7 Distributions of the transverse velocity component (v)

overlaid with the profile at ($x/\delta=100$). The similar features are also observed for other studied Reynolds numbers.

The friction coefficient ($C_f = 2\tau_w/\rho u_0^2$) for different Reynolds numbers is presented in Fig. 9. The friction coefficient decreases with the increase of Reynolds number. The friction coefficient becomes smaller from the inlet section and reaches the fully-developed values ($x/\delta > 100$). One feature in its distributions is that decrease of the friction coefficient in the streamwise direction does not follow the monotonous way in the entrance region. A minimum value is observed near the inlet section, which can be seen more clearly for the Reynolds number of 4560. Distributions of the bulk Nusselt number for different Reynolds numbers are shown in Fig. 10. The magnitude of Nusselt number increases with the increase of Reynolds number. The Nusselt number becomes smaller in its magnitude from the inlet section and approaches the fully developed values ($x/\delta > 120$). Similarly, the Nusselt number in the streamwise direction does not decrease monotonously in the entrance region. A minimum value in the

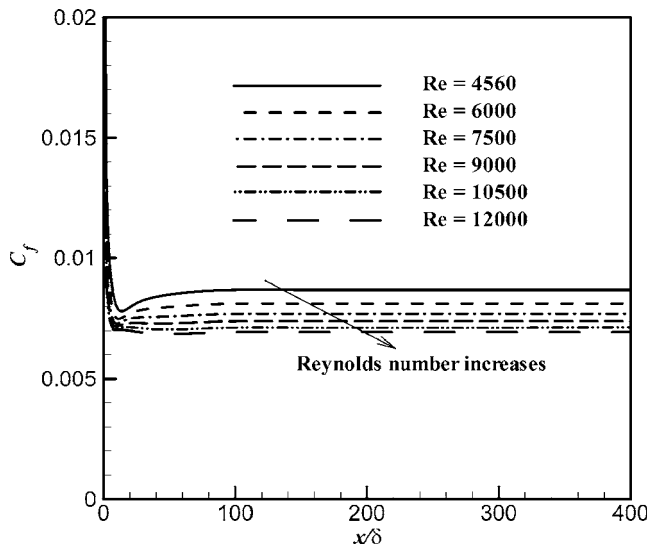


Fig. 9 Distributions of the friction coefficient (C_f)

streamwise distribution of the Nusselt number develops in the entrance region of turbulent convection channel flow for the studied Reynolds numbers

Conclusions

Convection in turbulent forced flow in a parallel channel, where the walls are heated with constant heat flux, is examined for the purpose of determining the flow and thermal behavior that simul-

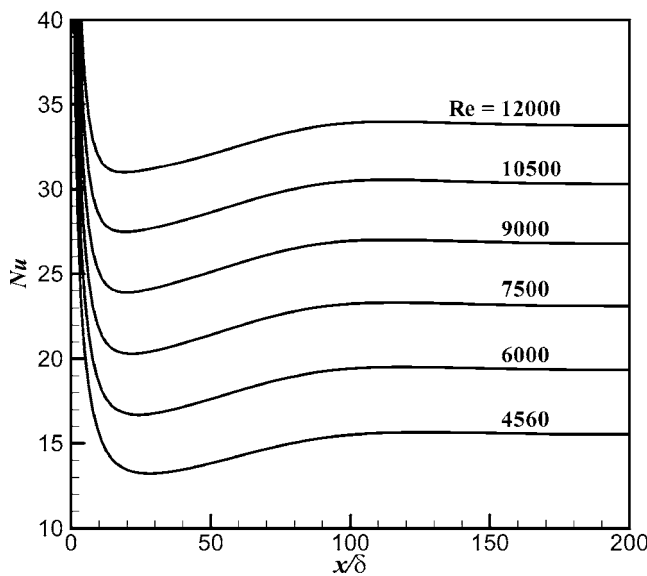


Fig. 10 Distributions of the bulk Nusselt number (Nu_b)

taneously develops in the entrance region of this geometry. Non-parabolic patterns in the mean streamwise velocity component are observed for the studied Reynolds numbers. The peak streamwise velocity component develops to appear near the wall, but not at the centerline, in the entrance region. Such patterns are also seen in the distribution of temperature field. The friction coefficient decreases with the increase of Reynolds number. The Nusselt number increases with the increase of Reynolds number. It does not reach the fully developed value monotonously and a minimum develops in the developing region.

Acknowledgment

This work was in part supported by U.S. Army Research Laboratory under Grant No. DAAD 19-03-2-0007 and by U.S. Department of Energy under Grant Nos. DE-FG02-03ER46067 and RF-05-HFS-006. J.H.N. gratefully acknowledges H. Lan for useful discussions.

References

- [1] Hussain, A. K. M. F., and Reynolds, W. C., 1975, "Measurements in Fully Developed Turbulent Channel Flow," *ASME J. Fluids Eng.*, **97**(4), pp. 568–580.
- [2] Wei, T., and Willmarth, W. W., 1989, "Reynolds-Number Effects on the Structure of a Turbulent Channel Flow," *J. Fluid Mech.*, **204**, pp. 57–95.
- [3] Johansson, A. V., and Alfredsson, P. H., 1982, "On the Structure of Turbulent Channel Flow," *J. Fluid Mech.*, **122**, pp. 295–314.
- [4] Kim, J., Moin, P., and Moser, R., 1987, "Turbulence Statistics in Fully Developed Turbulent Channel Flow at Low Reynolds Number," *J. Fluid Mech.*, **177**, pp. 133–166.
- [5] Moser, R. D., Kim, J., and Mansour, N. N., 1999, "Direct Numerical Simulation of a Fully Developed Turbulent Channel Flow Up to $Re_\tau=590$," *Phys. Fluids*, **11**(4), pp. 943–945.
- [6] Abe, H., Kawamura, H., and Matsuo, Y., 2000, "Direct Numerical Simulation of a Fully Developed Turbulent Channel Flow With Respect to the Reynolds Number Dependence," *ASME J. Fluids Eng.*, **123**(2), pp. 382–393.
- [7] Kim, J., and Moin, P., 1989, "Transport of Passive Scalars in a Turbulent Channel Flow," *Turbulent Shear Flow VI*, J.-C. Andre, J. Cousteix, F. Durst, B. E. Launder, F. W. Schmidt, and J. H. Whitelaw, eds., Springer, Berlin, pp. 85–96.
- [8] Kasagi, N., Tomita, Y., and Kuroda, A., 1992, "Direct Numerical Simulation of Passive Scalar Field in a Turbulent Channel Flow," *ASME J. Heat Transfer*, **114**(3), pp. 598–606.
- [9] Debusschere, B., and Rutland, C. J., 2004, "Turbulent Scalar Transport Mechanisms in Plane Channel and Couette Flows," *Int. J. Heat Mass Transfer*, **47**(8&9), pp. 1771–1781.
- [10] Abe, K., Kondoh, T., and Nagano, Y., 1994, "A New Turbulence Model for Predicting Fluid Flow and Heat Transfer in Separating and Reattaching Flows—I. Flow Field Calculations," *Int. J. Heat Mass Transfer*, **37**(1), pp. 139–154.
- [11] Abe, K., Kondoh, T., and Nagano, Y., 1995, "A New Turbulence Model for Predicting Fluid Flow and Heat Transfer in Separating and Reattaching Flows—II. Thermal Field Calculations," *Int. J. Heat Mass Transfer*, **38**(8), pp. 1467–1481.
- [12] Chen, Y. T., Nie, J. H., Armaly, B. F., and Hsieh, H. T., 2006, "Turbulent Separated Convection Flow Adjacent to Backward-Facing Step—Effects of Step Height," *Int. J. Heat Mass Transfer*, **49**(19&20), pp. 3670–3680.
- [13] Patankar, S. V., 1980, *Numerical Heat Transfer and Fluid Flow*, Hemisphere, New York.
- [14] Vogel, J. C., and Eaton, J. K., 1985, "Combined Heat Transfer and Fluid Dynamic Measurements Downstream of a Backward-Facing Step," *ASME J. Heat Transfer*, **107**(4), pp. 922–929.
- [15] Kays, W., and Crawford, M. E., 1980, *Convective Heat and Mass Transfer*, McGraw-Hill, New York.
- [16] Yu, B., and Ozoe, H., 2001, "Non-Parabolic Flow Pattern at the Entrance Region in a Circular Tube With a Uniform Inlet Velocity," *Numer. Heat Transfer, Part A*, **39**(8), pp. 857–862.